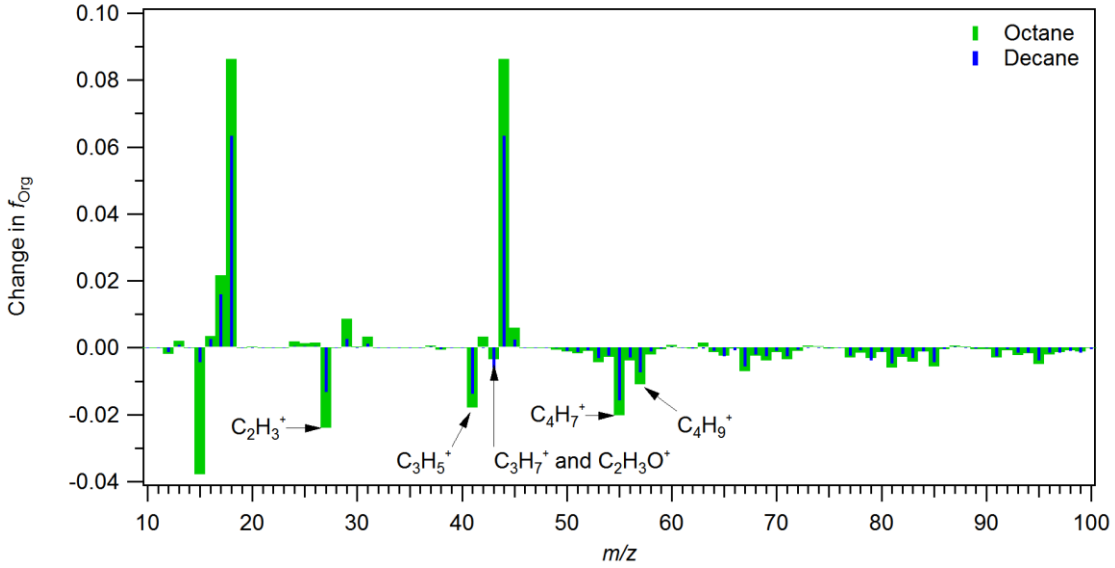

Figure S1: Change in the fractional contribution by different organic ion fragments to the overall organic aerosol mass as measured by the ACSM. Dodecane-Cl SOA (Exp. 11) was used as the reference for octane-Cl SOA (Exp. 3) and decane-Cl SOA (Exp. 7) produced under similar oxidation conditions under low RH. Mass spectra shown are 50-minute averages from minute 10 to 60 during the photooxidation period. Ion identities indicated ($C_2H_3^+$, $C_3H_5^+$, $C_3H_7^+$, $C_2H_3O^+$, $C_4H_7^+$, $C_4H_9^+$) were assumed, as the quadruple ACSM used lacks the necessary mass resolution for exact identification. At *m/z* 43, the $C_2H_3O^+$ is expected to dominate. Highlighted C_xH_y ions are often associated with hydrocarbon-like organic aerosol (Ng et al., 2011; Ulbrich et al., 2009). Clear enhancement of *m/z* 44 and associated ion fragments (e.g. *m/z* 16, 17, and 18) was also observed for octane and decane SOA.

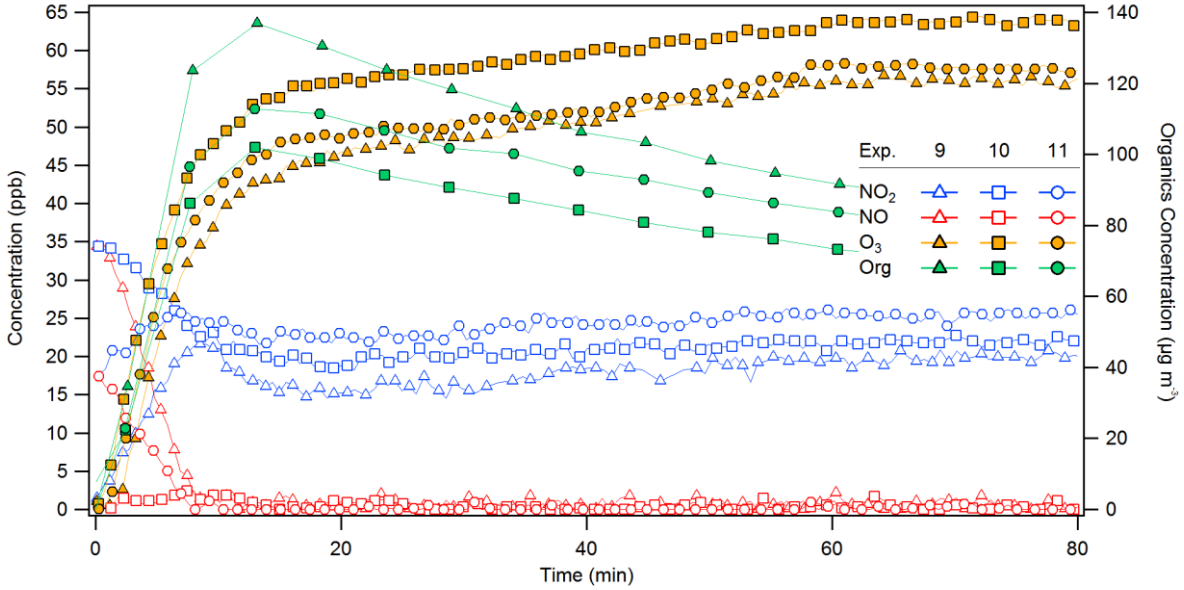

Figure S2: Example of NO, NO_2, O_3 and SOA trends under different starting NO_x conditions. Exp. 9 (high initial NO), 10 (high initial NO_2), and 11 (balanced initial NO and NO_2) for chlorine-initiated oxidation of dodecane under low RH conditions are shown. Ozone production slowed down significantly as the NO_x concentrations plateaued and as the SOA concentrations approached their maxima. By the end of the photooxidation period (60 min), lowest final NO_x concentrations (consisting of NO_2 and interferences, which may include alkyl nitrates) and highest SOA concentrations were observed for high initial NO concentrations (Exp. 1 for octane, Exp. 5 for decane, and Exp. 9 for dodecane).

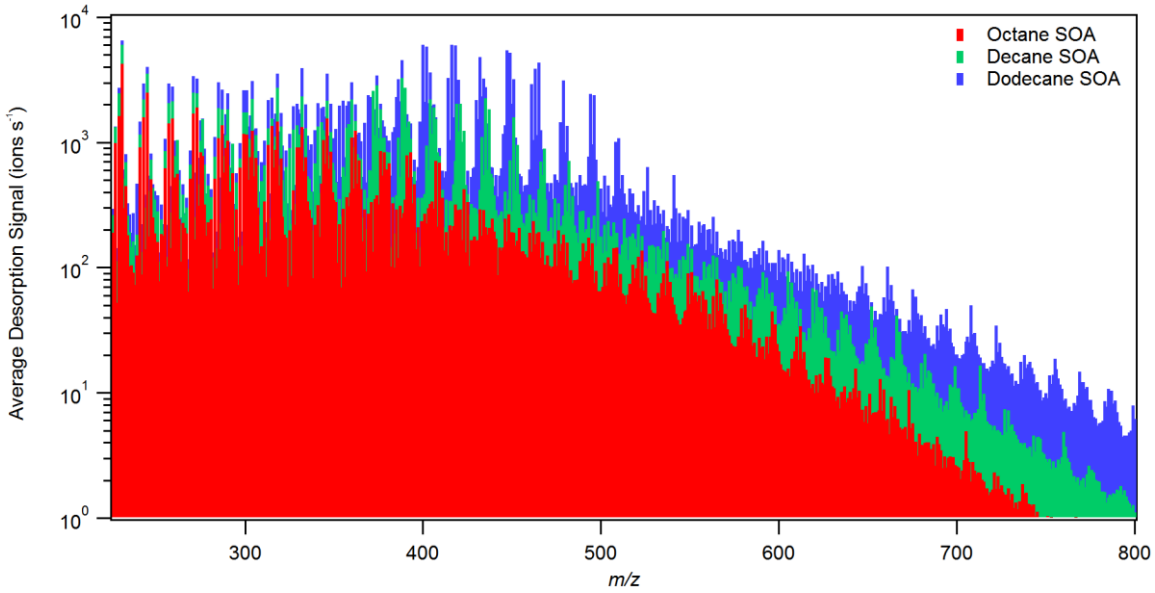

Figure S3: Comparison of particle-phase composition during FIGAERO desorption for octane (Exp. 3), decane (Exp. 7), and dodecane (Exp. 11). Same as Figure 4 in the main text but with the y-axis in logarithmic scale and the x-axis (*m/z*) extended to the maximum sampled range. Desorption signals are not stacked.

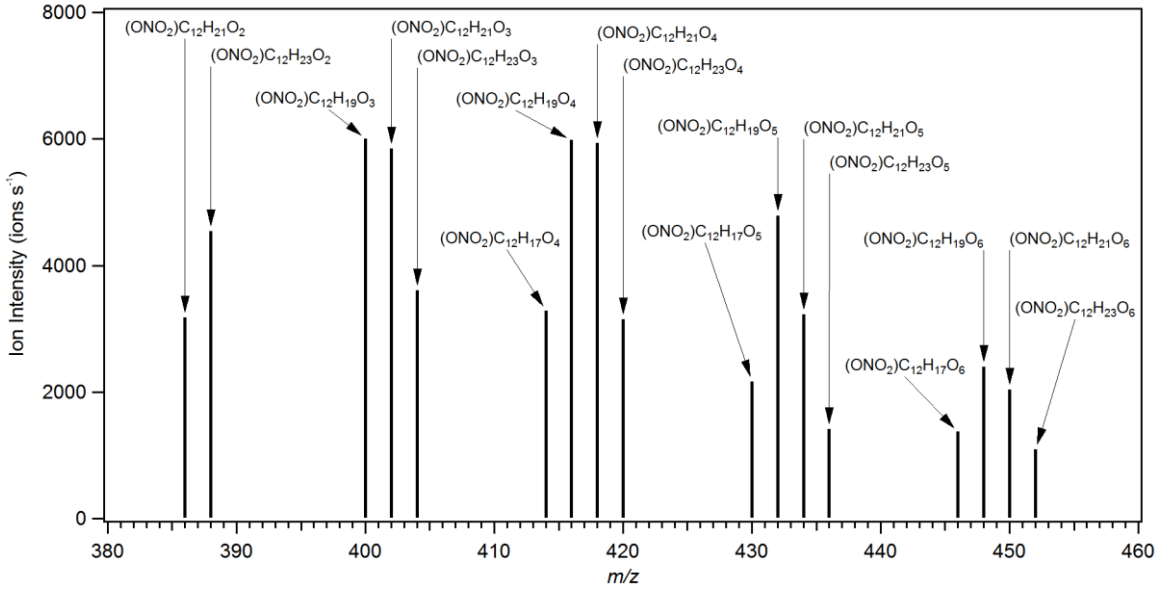

Figure S4: Particle-phase distribution of C_{12} organic (mono-)nitrates. Assuming equal sensitivity, the particle-phase abundance roughly followed a bell-shape distribution across the different oxygenation groups, peaking at the O_3 or O_4 group. Within each oxygenation group, the product distribution follows a bell-shape around H_{19} and H_{21} compounds. Similar bell-shaped organic nitrate distribution has been observed for ambient isoprene- and monoterpene-derived organonitrates (Lee et al., 2016).

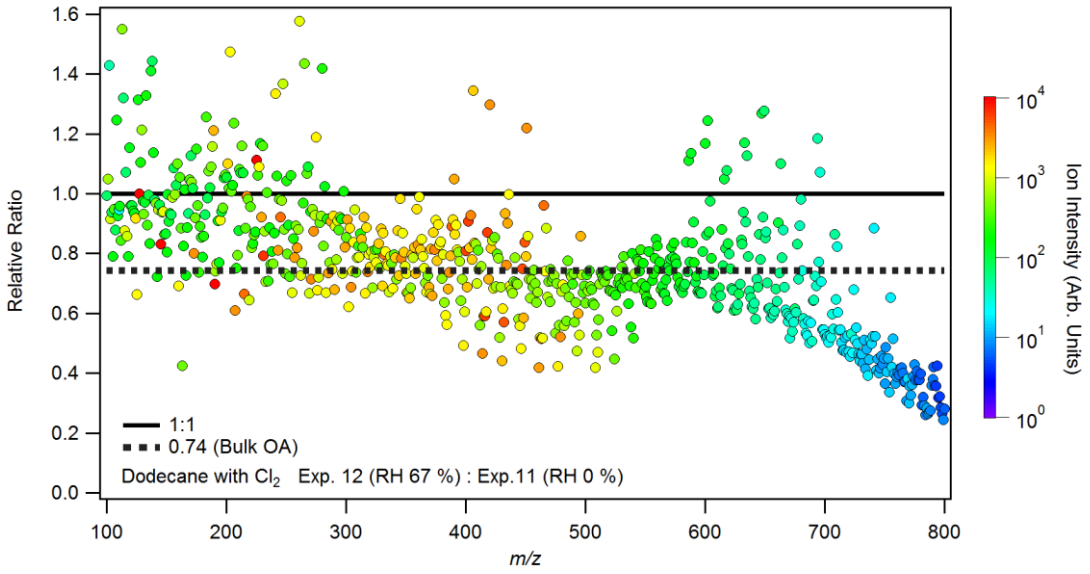

Figure S5: Ratio of integrated unit-mass resolution FIGAERO-CIMS desorption signal during temperature ramp from a high-RH SOA formation experiment (Exp. 12, 67 % RH) to that from a low-RH SOA formation experiment (Exp. 11, < 5 % RH). Integrated ion intensity is shown on a logarithmic scale as the color. The ratio of bulk organics concentration during the filter collection period calculated using ACSM data is shown as the dotted black line. Except for the low molecular weight thermal fragmentation/decomposition products and the high molecular weight, low-volatility compounds, the unit-mass ion ratios appear in agreement with bulk measurement. Under high RH conditions, the higher molecular weight (m/z > 600) compounds become increasingly suppressed.

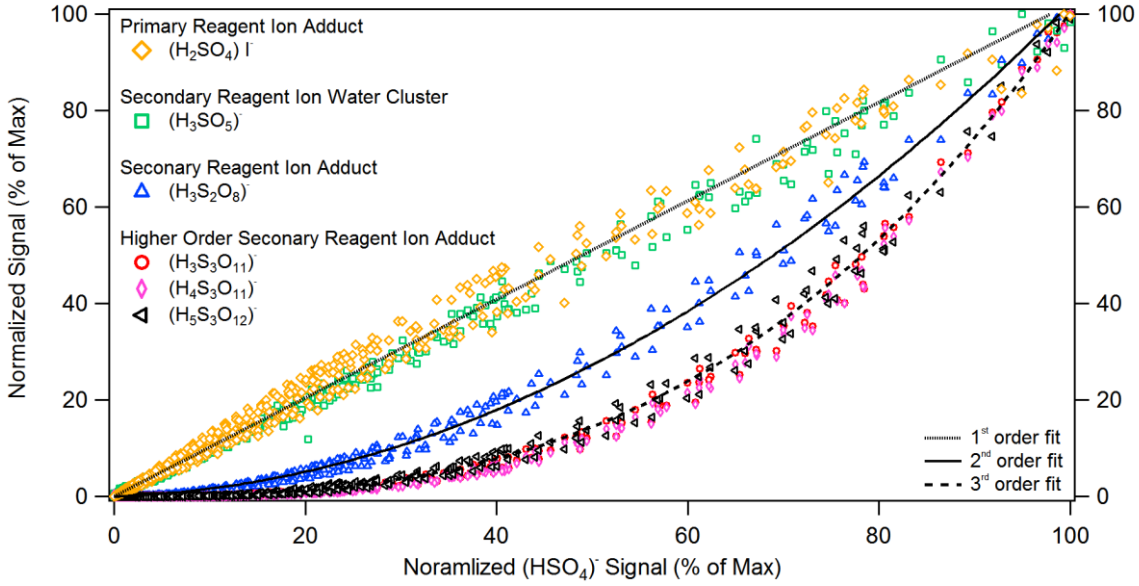

Figure S6: Example of secondary HSO_4^- ionization products. Ion signals observed during $(NH_4)_2SO_4$ thermal decomposition were first normalized by I^- signal and then normalized against the maximum desorption signal observed for each ion. Linear (1st order), quadratic (2nd order), and cubic equations (3rd order) are fitted.

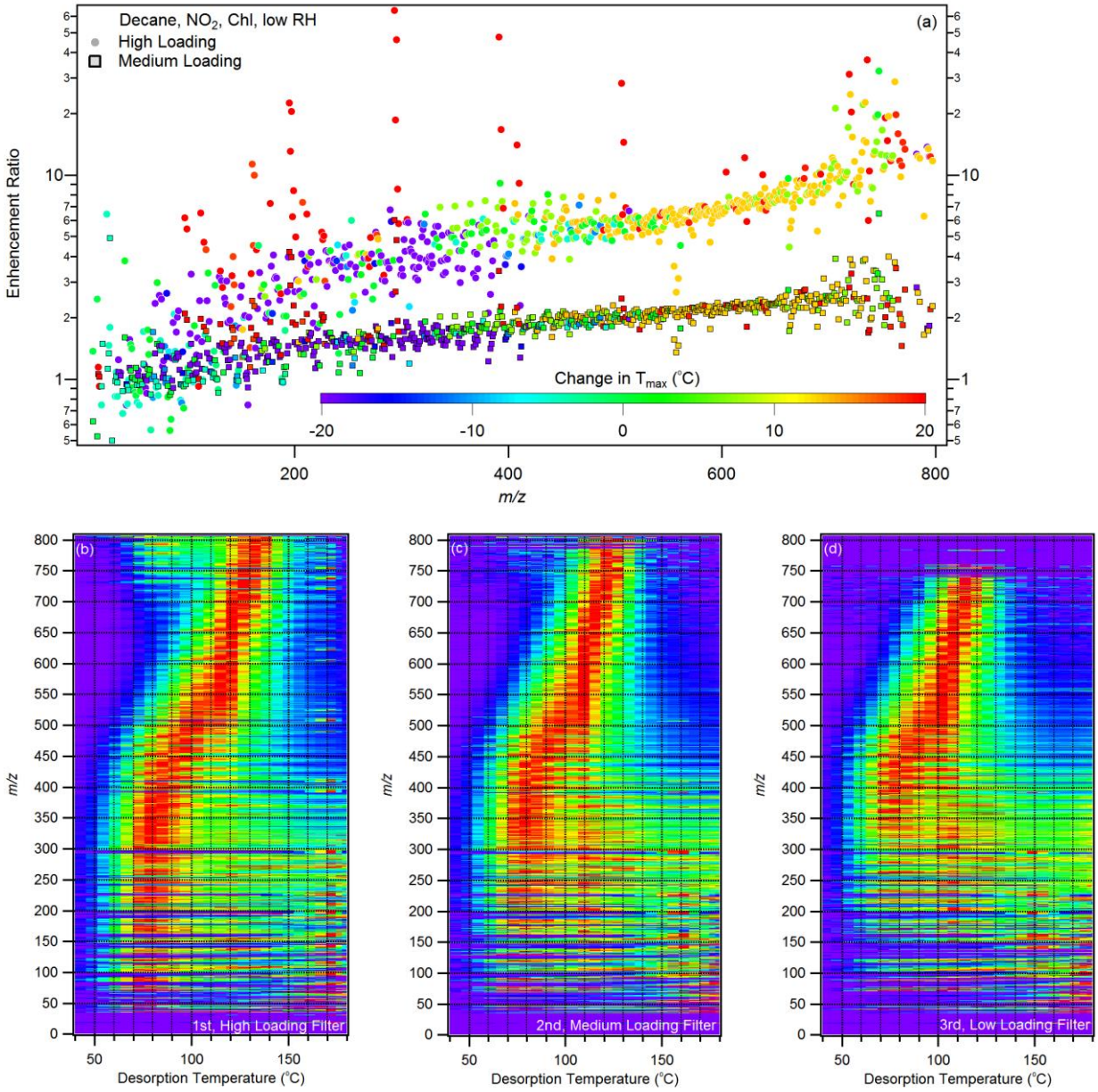

Figure S7: Effects of aerosol loading on T_{max} shift. Three SOA filter samples were collected during Exp. 6 for 45 mins, 30 mins, and 15 mins, in that order. Each filter was subjected to two full desorption runs to minimize carry-over effects and to determine the filter background. (a) Enhancement ratios calculated using unit-mass integrated signals for the lowest filter loading run as the referenced condition. Color scale shows T_{max} shifts in ºC, using the T_{max} values observed in the low loading run as the reference point. (b) 2-D thermogram for the first, high loading filter, (c) for the second, medium loading filter, and for (d) the third, low loading filter. For (b-d), the color scale represents the normalized desorption intensity as a percentage of the maximum, same as in Fig. 5 in the main text. Between the time it took for filter collection and filter desorption, the ion intensity of some high molecular weight, low volatility compounds had decreased to below the limits of detection (i.e. 3σ of the background signal) in the particle phase, likely due to volatility-dependent wall loss. Disappearance of low *m/z* (< 300) compounds maybe due to decreases in suspended aerosol concentration, making it unfavorable for semi-volatile compounds to partition to the particle phase, or may be associated with the loss of high molecular weight oligomers, assuming that the low *m/z* desorption ions were dominated by low-temperature (T_{max} < ~80 ºC) thermal fragmentation products as opposed to semi-volatile monomers.

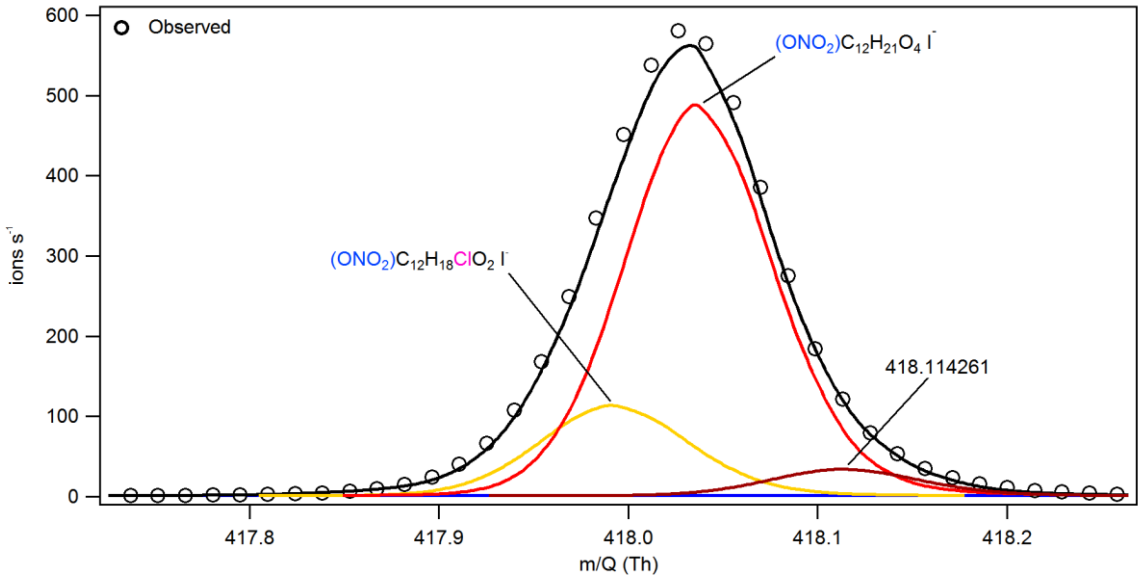

Figure S8: High resolution fitting at *m/z* 418 for Exp. 11. The C_{12} chloronitrate (ONO_2-$C_{12}H_{18}ClO_2$•I^-) peak is tentatively identified but it is buried in the shoulder of the nearby organonitrate (ONO_2-$C_{12}H_{21}O_4$•I^-) peak, which is much stronger. Because the chloronitrate peak is a weaker peak with significant overlap with a stronger peak, quantitative assessment would be challenging due to peak fitting uncertainties (Cubison and Jimenez, 2015). "418.114261" represents an unknown (possibly non-adducted) ion.

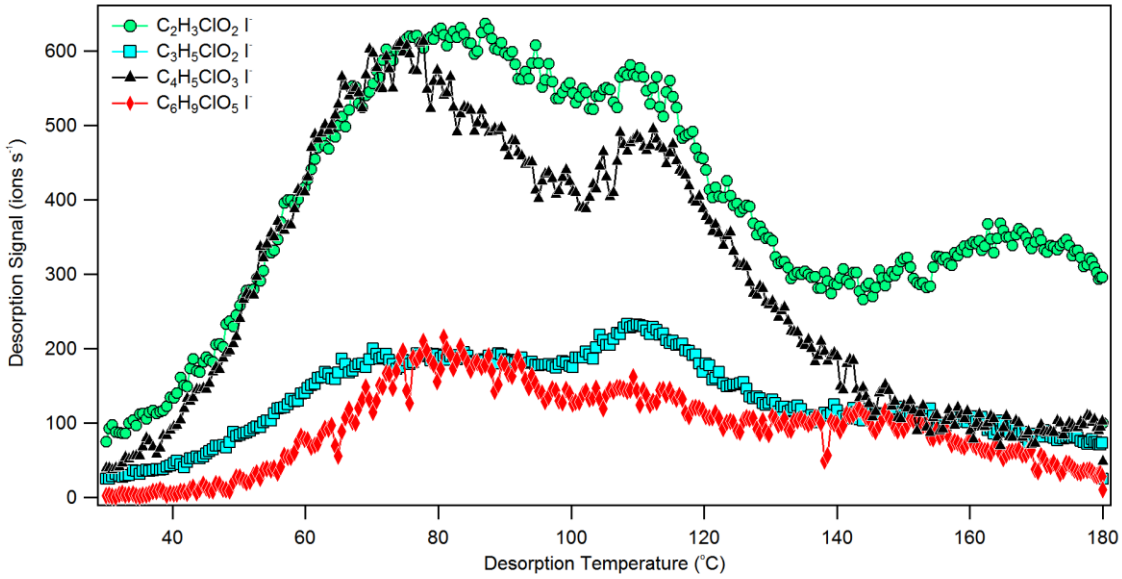

Figure S9: 1-D thermogram of select organochlorides observed for Exp 10. All compounds shown exhibited multimodal desorption behaviors. $C_2H_3ClO_2$ is too volatile to be present as a molecular compound in the particle phase and is therefore a thermal decomposition product. $C_2H_3ClO_2$ shows three local maxima at ~87 °C, ~109 °C, and ~167 °C. The T_{max} for the least volatile desorption mode of $C_2H_3ClO_2$ is higher than that for ammonium sulfate seed particles (~155 °C) from the same filter run, and may be produced from thermal decomposition of extremely low volatility organochlorides. However, larger organochloride ions were not observed to have any distinct T_{max} modes over these very high temperature ranges (> 160 °C)

References

Cubison, M. J. and Jimenez, J. L.: Statistical precision of the intensities retrieved from constrained fitting of overlapping peaks in high-resolution mass spectra, Atmos. Meas. Tech., 8(6), 2333–2345, doi:10.5194/amt-8-2333-2015, 2015.

Lee, B. H., Mohr, C., Lopez-Hilfiker, F. D., Lutz, A., Hallquist, M., Lee, L., Romer, P., Cohen, R. C., Iyer, S., Kurtén, T., Hu, W., Day, D. A., Campuzano-Jost, P., Jimenez, J. L., Xu, L., Ng, N. L., Guo, H., Weber, R. J., Wild, R. J., Brown, S. S., Koss, A., de Gouw, J., Olson, K., Goldstein, A. H., Seco, R., Kim, S., McAvey, K., Shepson, P. B., Starn, T., Baumann, K., Edgerton, E. S., Liu, J., Shilling, J. E., Miller, D. O., Brune, W., Schobesberger, S., D'Ambro, E. L. and Thornton, J. A.: Highly functionalized organic nitrates in the southeast United States: Contribution to secondary organic aerosol and reactive nitrogen budgets, Proc. Natl. Acad. Sci., 113(6), 201508108, doi:10.1073/pnas.1508108113, 2016.

Ng, N. L., Canagaratna, M. R., Jimenez, J. L., Zhang, Q., Ulbrich, I. M. and Worsnop, D. R.: Real-time methods for estimating organic component mass concentrations from aerosol mass spectrometer data, Environ. Sci. Technol., 45(3), 910–916, doi:10.1021/es102951k, 2011.

Ulbrich, I. M., Canagaratna, M. R., Zhang, Q., Worsnop, D. R. and Jimenez, J. L.: Interpretation of Organic Components from Positive Matrix Factorization of Aerosol Mass Spectrometric Data., Atmos. Chem. Phys., 9, 2891, doi:10.5194/acp-9-2891-2009, 2009.